BEAM DYNAMICS IN A HELIX LINEAR ACCELERATOR FOR HEAVY IONS

J. Klabunde, H. Deitinghoff, H.P. Junior, H. Klein
Institut für angewandte Physik der Universität
Frankfurt/Main, Germany

ABSTRACT

Beam dynamics in a helix linear accelerator is treated in the following way:

In the first instance the uncoupled equations of motion, corresponding to the synchronous particle, are used for the choice of the focusing device and the determination of quadrupole field gradients, giving maximum radial acceptances.

The transverse and axial acceptances are then computed by using the general expressions for particle motion. Effects of coupling and non-linearities are considered.

Energy spread and phase width of the particle bunches are calculated for different final energies of ions. The problem of energy variation, the simultaneous acceleration of differently charged ions, the maintenance of good time structure of the beam within a wide energy range and the possibility of increasing the final energy for ions with higher charge-to-mass ratio are presented.

I. Introduction

The helical waveguide has been investigated theoretically and experimentally in our institute.[1,2] The results of this work demonstrate that the helix structure is well suited for the acceleration of heavy ions. The particle dynamics in a helix linear accelerator differs appreciably from that in conventional linacs. The electromagnetic fields of the helix, the arrangement of accelerating and focusing elements require the modification of existing and the development of new methods. There is more flexibility in the choice of parameters for the axial and radial motion than with a conventional drift-tube structure. Furthermore the specific problems of the acceleration of heavy ions have to be taken into consideration.

II. Fundamental Considerations

The accelerating structure consists of a helical waveguide, surrounded by a cylindrical outer conductor. An rf wave moves along the helical wire with about the speed of light generating an electric field on the axis. It has a longitudinal component, sinusoidally varying with time and axial direction. The parameters of the helix have to be chosen in such a manner that the phase velocity of the rf wave on the axis is lowered in order to obtain continuous acceleration of heavy ions. Only

the radial and axial electric fields have to be considered for the particle dynamics since the other field components are weak.

The basic scheme of the helix accelerator is shown in Fig. 1. The linac is divided into sections, the length of each section is about 1 m. The focusing elements are placed between the sections. The advantages of this arrangement for the flexibility of the helix linac are discussed in this paper.

Each section is excited in standing wave mode. The equations of motion for standing and travelling waves are cited in Fig. 2.

The backward wave in the standing wave operation will induce small oscillatory perturbations on the phase and energy. The influence of the backward wave will be neglected in the following discussions. Only the equations of motion for the travelling wave are considered.

A proposal for a heavy ion accelerator with the helix structure was submitted.[3] The relevant parameters of this proposal are shown in Fig. 3.

The helix accelerator starts with an injection energy of 0.130 MeV/N. This energy corresponds to a necessary total accelerating voltage of 2.8 MV for U^{11+}-ions. The helix prestripper linac consists of 30 sections; synchronous acceleration of ions with low charge-to-mass ratio (0.046) takes place at 27.12 MHz. The poststripper linac accepts ions with a charge-to-mass ratio ≥ 0.105. This can be achieved by a gasstripper. The rf frequency is increased to 108.48 MHz.

A final energy of 7 MeV/N is obtained with 45 helix sections. The final energy can be increased to 8.5 respectively 10 MeV/N with further 10 respectively 21 sections.

The radial focusing is provided by magnetic quadrupole doublets in the prestripper part and by singulets in the poststripper linac.

III. Particle Dynamics - Synchronous Acceleration

An analytical solution of the system of differential equations for the particle motion does not exist. At first the linearized equations of motion are solved. In this approximation the transverse and longitudinal motions are uncoupled. The radial motion for the synchronous particle is described by the equation

$$\ddot{r} + K^2 r = 0$$

where K is in the helix

$$K_W^2 = \frac{\zeta}{N} \cdot \frac{e}{2m} \cdot k\, E \sin \varphi_s$$

and in the quadrupoles

$$K_m^2 = \pm \frac{\zeta}{N} \cdot \frac{e}{m} \cdot \frac{v_s}{c} \cdot B'$$

(φ_s = synchronous phase, B' = magnetic field gradient; further definitions see Fig. 2)

As the consequence of the constant helix lengths the linac is not periodic contrary to drift-tube structures. The flight times of the particles decrease from section to section.

The AG-theory as developed in the theory of strong focusing synchrotrons is used.[4] A comparison with exact numerical computations shows that this formalism gives good qualitative informations.[4,5]

The stability diagrams can be used in order to estimate the range of the stable radial motion. Fig. 4 shows a stability diagram for the singulet focusing device. The parameters are

$$\Delta = K_W^2 \cdot \frac{L_W^2}{v_s^2}$$

$$\Theta_o^2 = K_m^2 \cdot \frac{L_Q^2}{v_s^2}$$

(v_s = velocity of the synchronous particle, L_W = helix length, L_Q = quadrupole length)

The influence of different parameters on the radial motion may be derived from the stability diagrams.

Fig. 5 shows the acceptance and the magnetic field gradients for the poststripper part (parameter see Fig. 3). The acceptance considerably increases along the linac. This statement was confirmed by exact computation of the acceptances.

A computer program has been developed in order to optimize the magnetic field gradients with respect to maximum radial acceptances and tolerances.[6] With these magnetic gradients the exact transverse and longitudinal acceptances are calculated numerically. Non-linearities and coupling of transverse and longitudinal motion are included. The mechanism for coupling consists of 1) the dependence of the transverse rf defocusing impulse on the longitudinal phase and 2) the dependence of the energy gain on transverse displacement.

The computer programs are extensively discussed in [5].

The radial acceptance areas of the prestripper and poststripper accelerator are shown in Figs. 6 and 7 for various starting conditions $\Delta\varphi$, ΔT. The acceptance areas of the various phase and energy deviations do not differ much. The acceptance of the prestripper linac was estimated to 58 cm mrad (T = 0.130 MeV/N, aperture = 4 cm, magnetic field gradients: 1.9 - 3.5 kG/cm); the acceptance of the poststripper part is 30 cm mrad (T = 1.4 MeV/N, aperture = 4 cm, gradients: 1.5 - 2.2 kG/cm). The acceptance can be increased to 50 cm mrad when this part starts with helix sections of 60 cm length.

Figs. 6 and 7 show that the slope of the acceptances in that plane, in which the first lens is focusing, is more sensitive to a change of

the initial values in the longitudinal phase space.

The longitudinal acceptances of axial particles are shown in Figs. 8 and 9. The acceptances also are computed for a comparison without drift length between adjacent sections. The "fish-shaped" longitudinal acceptance is determined without considering the variation of the parameters along the linac.

The couplings between transverse and longitudinal motion cause a deterioration of beam quality. The effect on transverse emittance is shown in Fig. 10. For a collection of starting values of longitudinal phase space there is an apparent increase of the radial emittance.

The longitudinal emittance is calculated by a computer program. In this case a block of particles with $\Delta\varphi$, ΔT -coordinates($r = \dot{r} = 0$) is sent into the linac. The energy-phase space distribution, energy and phase spectra are calculated.An example is given in Fig. 11 for U^{25+}. Further computational results are given in table 1.

Figs. 12 and 13 show that simultaneous multicharge acceleration behind the stripper is possible. Phase and energy spread of the output beam increase. Ions with different charge state are well focused. The helix and the focusing device being adjusted to U^{25+}.

IV. Non-Synchronous Acceleration

The arrangement of helix sections offers many advantages. The particle velocity has not to correspond necessarily with the phase velocity of the electric wave; the particle energy can vary in a certain range. The width of this range is limited by the decreasing rf efficiency for non-synchronous particles. The efficiency may be described with the transit-time factor:

$$Z = \frac{\sin\{\omega \cdot \frac{L}{2} \cdot (\frac{1}{v_T} - \frac{1}{v_{ph}})\}}{\omega \cdot \frac{L}{2} \cdot (\frac{1}{v_T} - \frac{1}{v_{ph}})}$$

The value $Z(\leq 1)$ gives that fraction of the maximum field which is useful as average axial field for non-synchronous acceleration.

Fig. 14 shows some curves of the transit-time factor for different parameters.

The rf action on the beam vanishes below 4 and beyond 16 MeV/N for sections of 1 meter which are designed for 7 MeV/N synchronous acceleration. These limits estimate the range of energy variation with maintenance of good microstructure (see table 1) and the attainable maximum energies for ions with high ζ/N-values. The maximum energy is plotted versus the atomic mass number in Fig. 15. The computational results of the energy spread and pulse width for different energies are listed in table 1.

As the fractional increase in the velocity of the ions in a section is relative small, it is possible to make the phase velocity constant throughout one or more sections. This simplifies the fabrication of the helix sections. The particle dynamics in this case has been extensively investigated.[5] The differences to the synchronous acceleration treated in chapter III are small.

V. Post-Acceleration With Helix Linac

The helix structure may be used for extensions of tandem or other low energy machines. A helix accelerator has been proposed for increasing the energy of a tandem accelerator (Emperor). The parameters of this machine are given in [2]. Ions with a minimum charge-to-mass ratio q = 0.28 are accepted (Bromine, ζ = 23).

The radial focusing is provided by magnetic singulets (N = 1); the radial acceptance was calculated to 24.6 cm mrad (normalized acceptance 1.27 cm mrad). The final energy for ions with a higher charge-to-mass ratio is shown in Fig. 16.

Acknowledgement

The computations have been carried out at the Zentrales Recheninstitut of the Frankfurt university. The work has been supported by the Bundesministerium für Bildung und Wissenschaft.

References

1. Klein, H., Habilitationsschrift unpubl. (1968)
2. Klein, H., 1970 Proton Linear Accelerator Conference, NAL, Batavia (these proceedings)
3. Klein, H., Junior, P., Klabunde, J., Siart, O., Deitinghoff, H., Finke, P., Schempp, A., Proc. Int. Conf. Nucl. React. Induced by Heavy Ions, Heidelberg, 540 (1970, North Holland)
4. Junior, P., Habilitationsschrift unpubl. (1969)
5. Klabunde, J., Dissertation unpubl. (1970)
6. Junior, P., Deitinghoff, H., J. Comp. Phys. 5, 1 (1970)

Table I

Energy resolution and microstructure for uranium at various final energies

Final energy	Energy resolution ($\Delta T/T \times 10^3$)	Pulse width of particle bunches [nsec]
7.0	2.0	0.25
7.0 (with debunching)	0.2	1.4
7.0 ($\zeta = 23-27$)	6.0	0.8
6.0	3.0	0.12
5.1	1.4	0.28
4.5	2.1	0.33
3.0 +)	2.5	0.40
9.5 ++)	2.2	0.20
8.5 +++)	2.3	0.20
10.0 +++)	2.2	0.14
9.2 ++++)	2.3	0.28

+) Decreasing of helix lengths from 4.5 MeV/N from 1.0 to 0.6 m

++) Second stripper (foil) at 4.5 MeV/N; $\zeta = 54$

+++) With additional 10 resp. 21 sections

++++) Foilstripper at 1.4 MeV/N $\zeta_{Uranium} = 45$

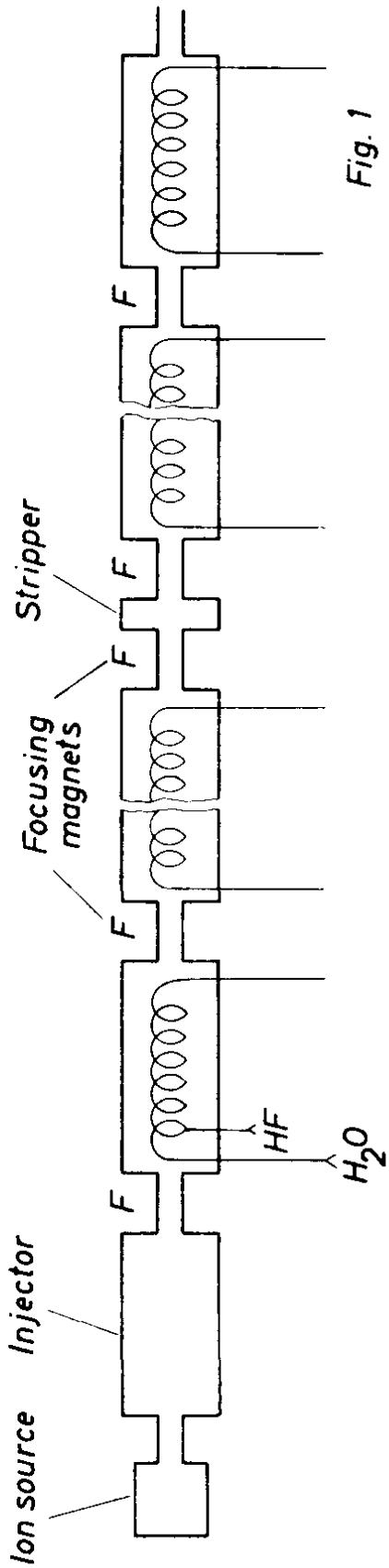
Ion source
Injector
Stripper
Focusing magnets
F
F
F
F
F
HF
H_2O

Fig. 1

Equations of motion:

1) Travelling wave

$$m\ddot{z} = \zeta \cdot e \cdot E \cdot I_0(\gamma r) \cdot \cos\left(\omega t - \int_0^z k\,dz' - \varphi\right)$$

$$m\ddot{r} = -\zeta \cdot e \cdot E \cdot \frac{k}{\gamma} \cdot I_1(\gamma r) \cdot \sin\left(\omega t - \int_0^z k\,dz' - \varphi\right)$$

2) Standing wave

$$m\ddot{z} = \zeta \cdot e \cdot 2E \cdot I_0(\gamma r) \cdot \cos(\omega t - \varphi) \cdot \cos \int_0^z k\,dz'$$

$$m\ddot{r} = -\zeta \cdot e \cdot 2E \cdot \frac{k}{\gamma} \cdot I_1(\gamma r) \cdot \cos(\omega t - \varphi) \cdot \sin \int_0^z k\,dz'$$

I_0, I_1 : Besselfunctions

E : Maximum electric field on the axis

$k = \frac{2\pi}{\lambda} = \frac{\omega}{v_{ph}}$, $k_0 = \frac{2\pi}{\lambda_0} = \frac{\omega}{c}$

$\gamma^2 = k^2 - k_0^2$

λ : Wavelength on the axis

λ_0 : Vacuum wavelength

ζ : Charge state of the ion

Fig. 2

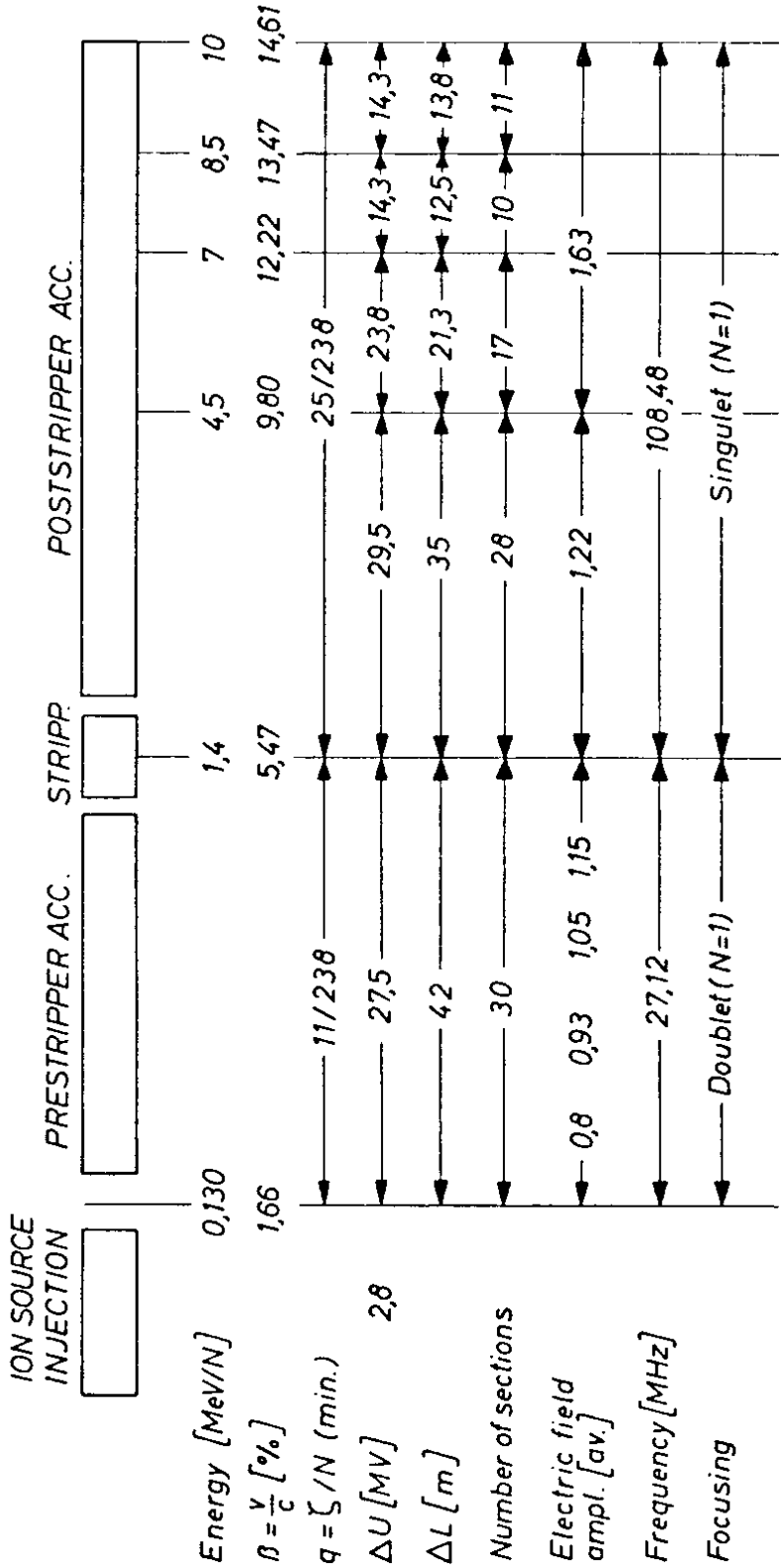
ION SOURCE INJECTION
PRESTRIPPER ACC.
STRIPP.
POSTSTRIPPER ACC.
Energy [MeV/N]
0,130
1,4
4,5
7
8,5
10
1,66
5,47
9,80
12,22
13,47
14,61
β = v/c [%]
q = ζ/N (min.)
11/238
25/238
ΔU [MV]
2,8
27,5
29,5
23,8
14,3
14,3
ΔL [m]
42
35
21,3
12,5
13,8
Number of sections
30
28
17
10
11
Electric field ampl. [av.]
0,8
0,93
1,05
1,15
1,22
1,63
Frequency [MHz]
27,12
108,48
Focusing
Doublet (N=1)
Singulet (N=1)

Fig. 3

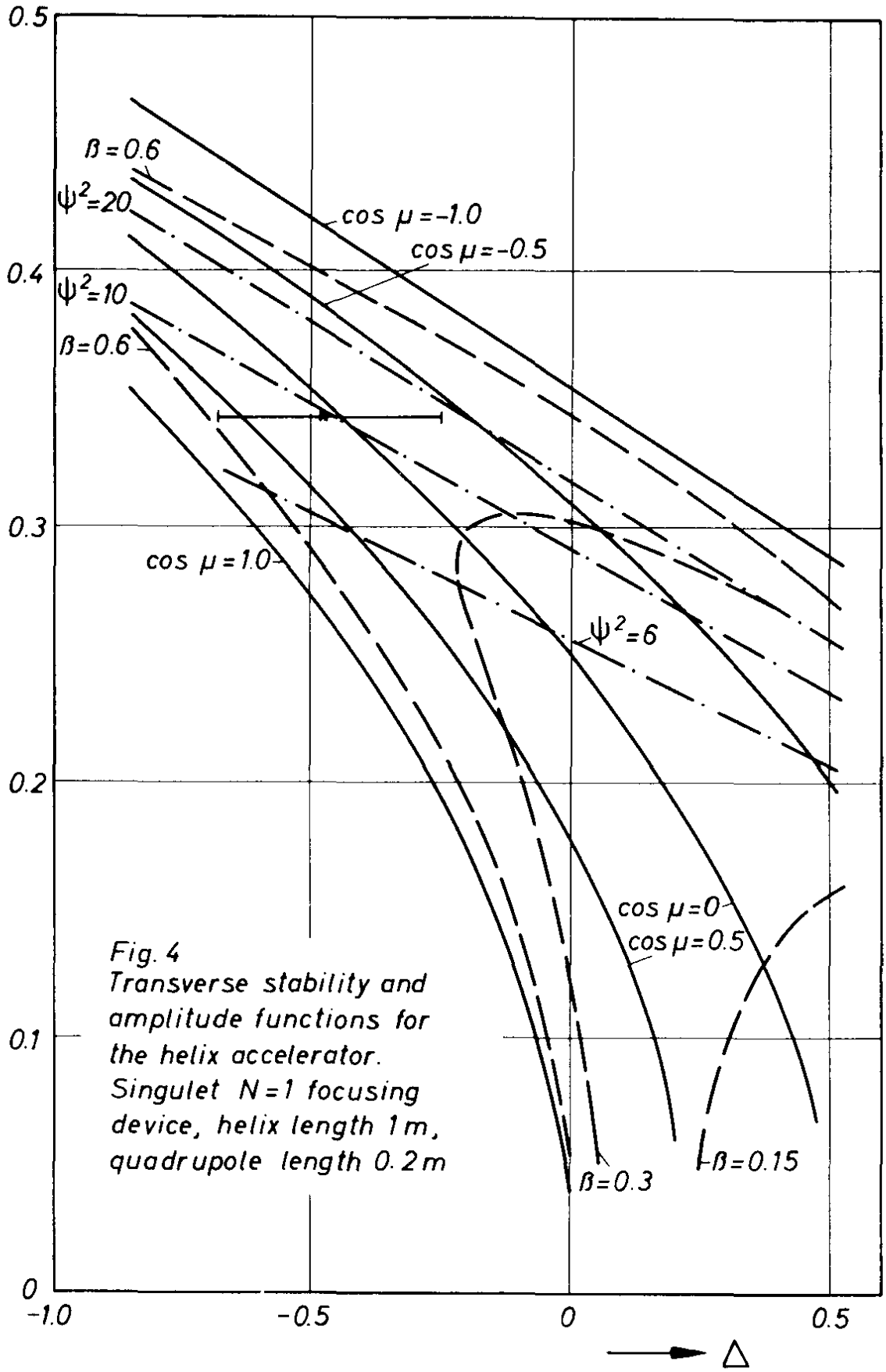

Fig. 4
Transverse stability and amplitude functions for the helix accelerator. Singulet N = 1 focusing device, helix length 1 m, quadrupole length 0.2 m

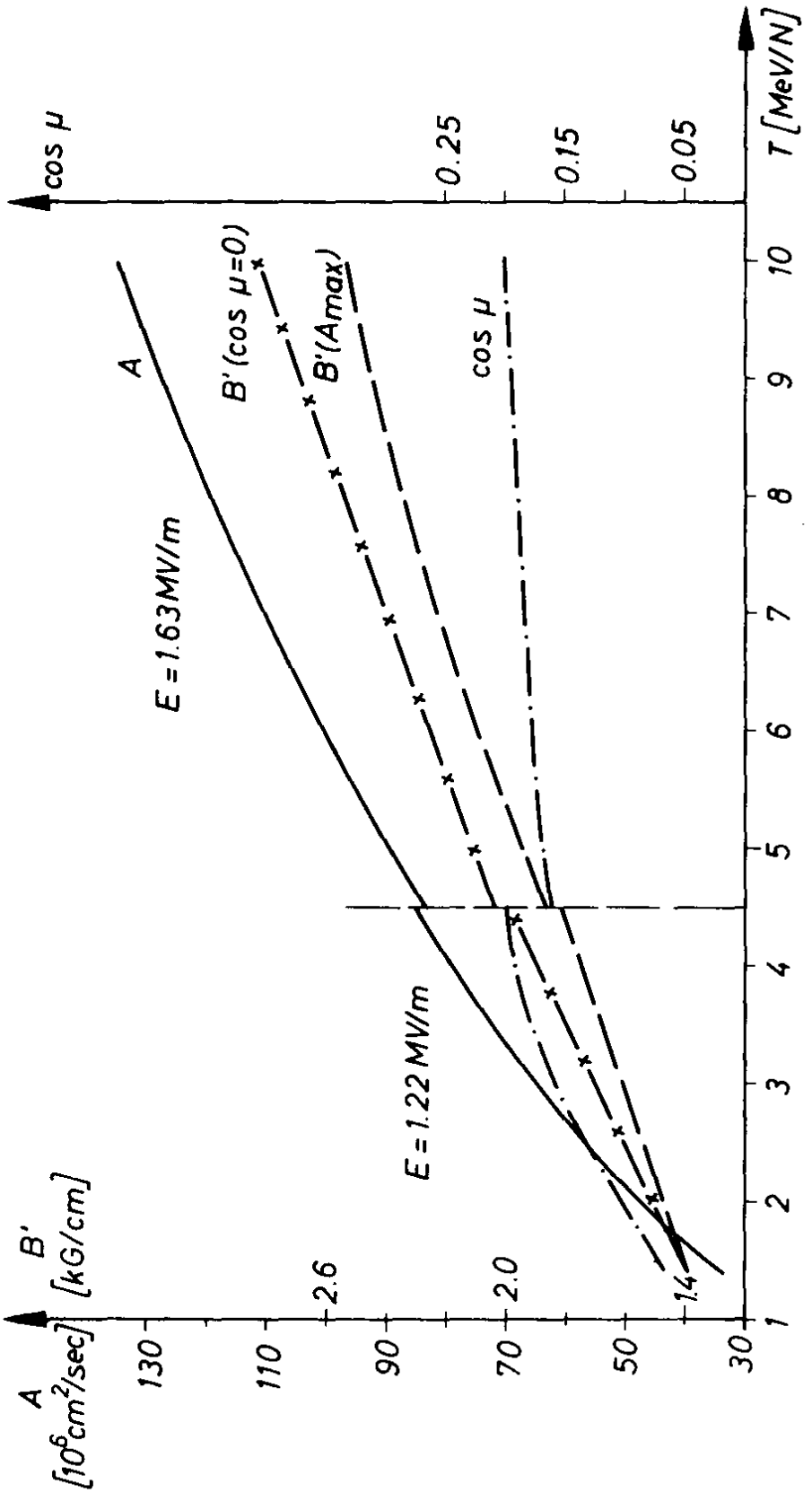

Fig. 5
Increased acceptance and field gradients along the helix linac.
(Helix length 1.0 m, quadrupole length 0.2 m, aperture 4 cm, f = 108.48 MHz)

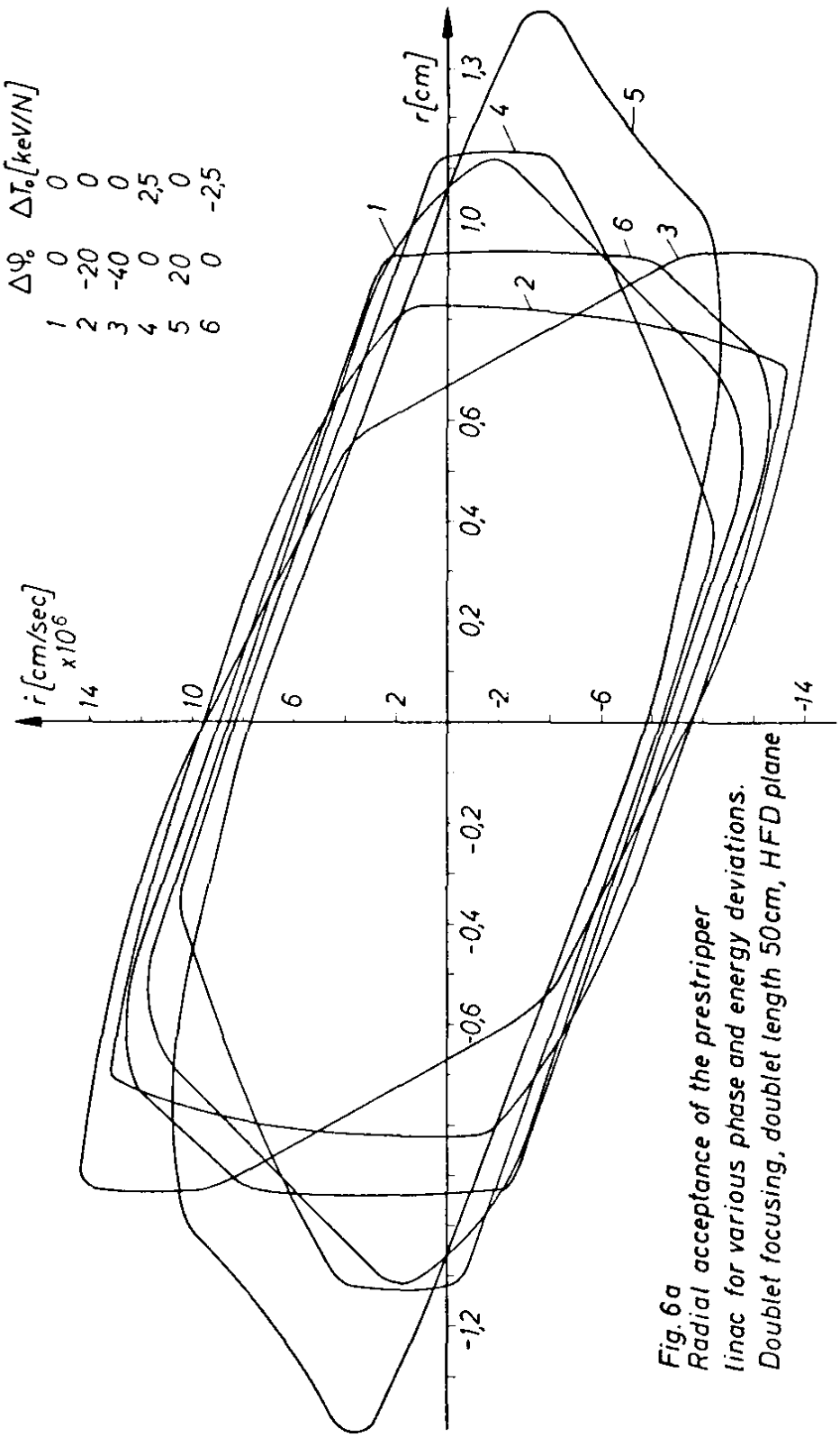

Fig. 6a
Radial acceptance of the prestripper linac for various phase and energy deviations. Doublet focusing, doublet length 50cm, HFD plane

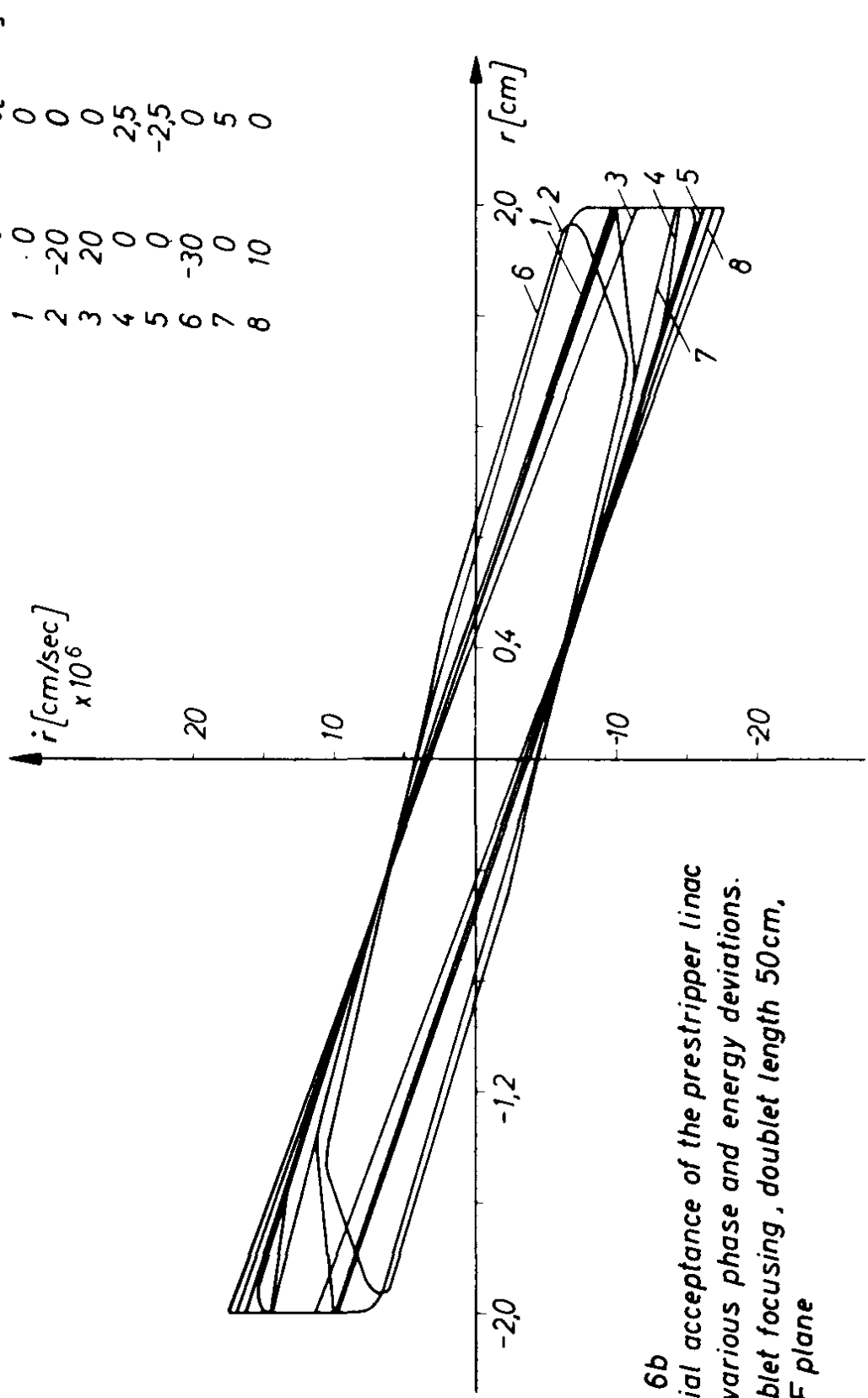

Fig. 6b
Radial acceptance of the prestripper linac for various phase and energy deviations. Doublet focusing, doublet length 50cm, HDF plane

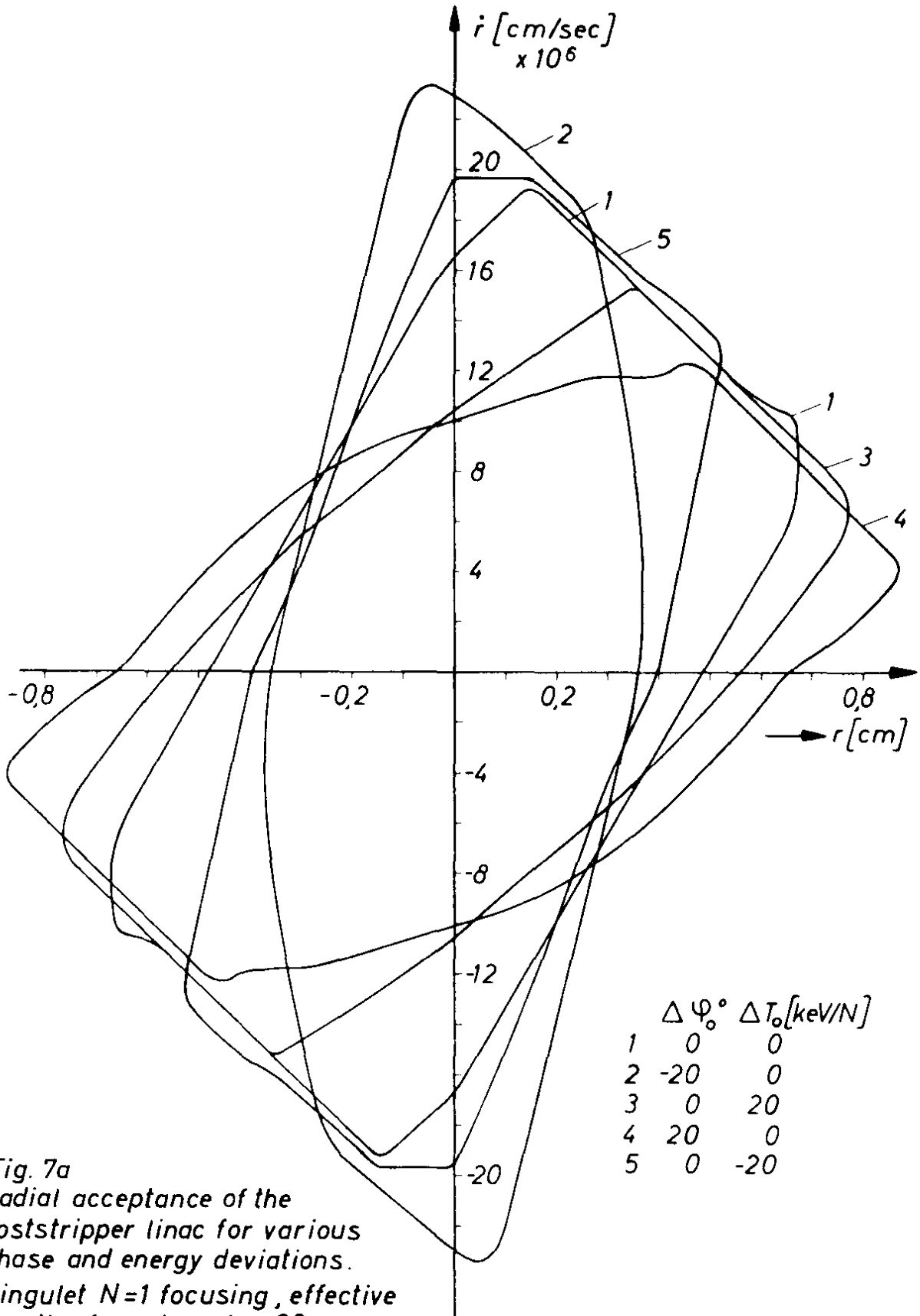

Fig. 7a
Radial acceptance of the poststripper linac for various phase and energy deviations.
Singulet N=1 focusing, effective length of quadrupoles 20 cm, HFHD plane

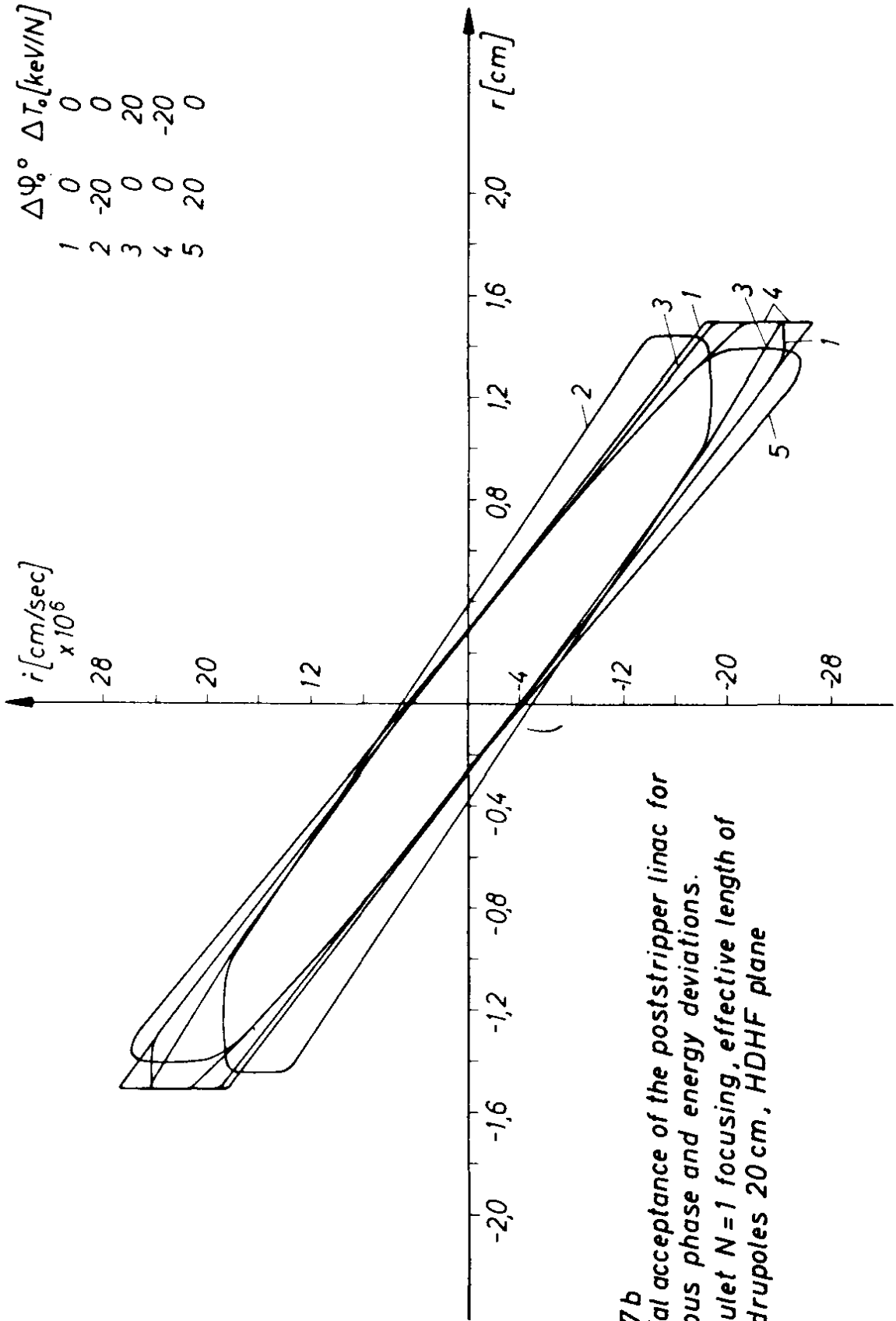

Fig. 7b
Radial acceptance of the poststripper linac for various phase and energy deviations.
Singulet N=1 focusing, effective length of quadrupoles 20 cm, HDHF plane

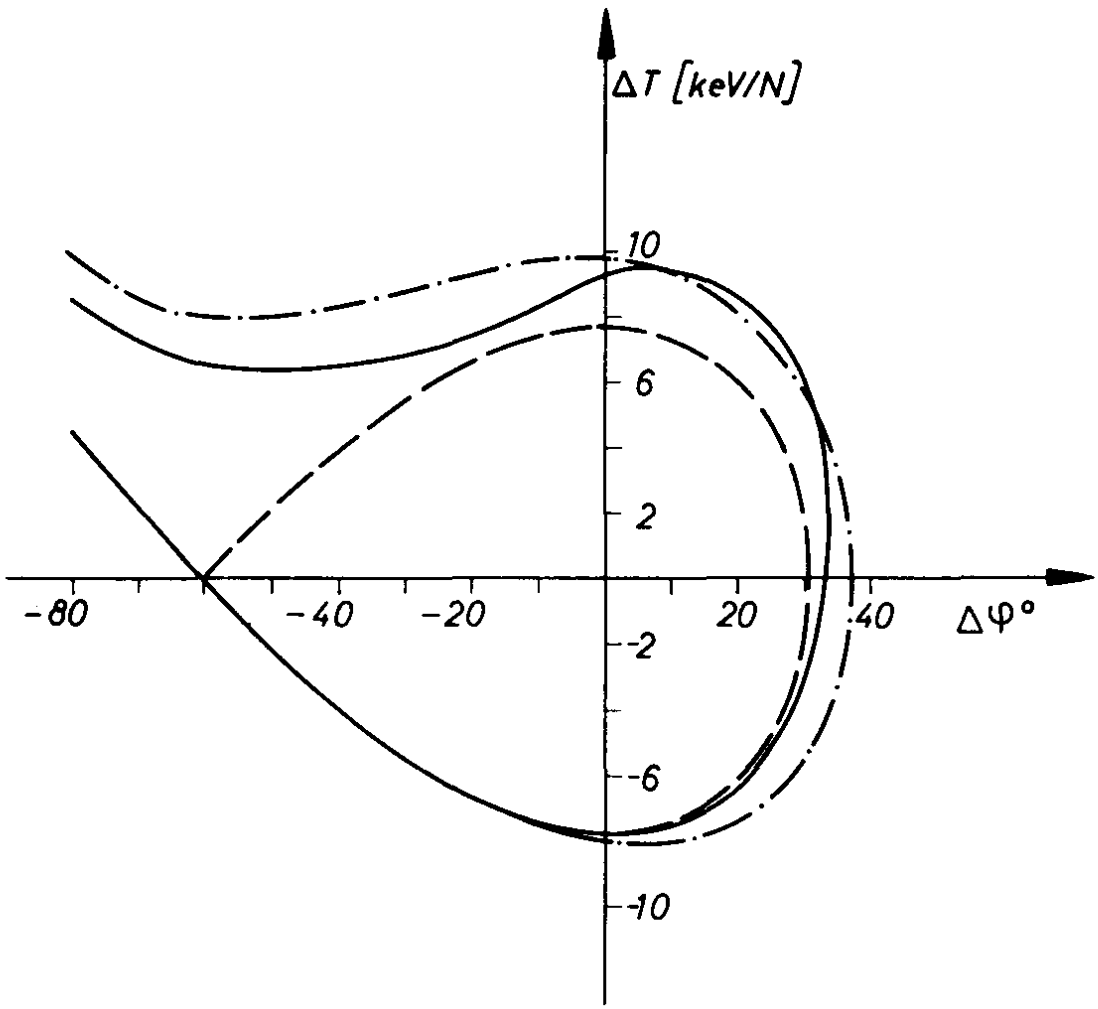

Fig. 8
Longitudinal acceptance of the poststripper accelerator for Uranium U^{11+}, $T_{initial} = 0.13 MeV/N$

— — — Approximative calculation (stationary potential method)

——— Exact computation, drift length 50 cm

—·—·— Exact computation, without drift lengths

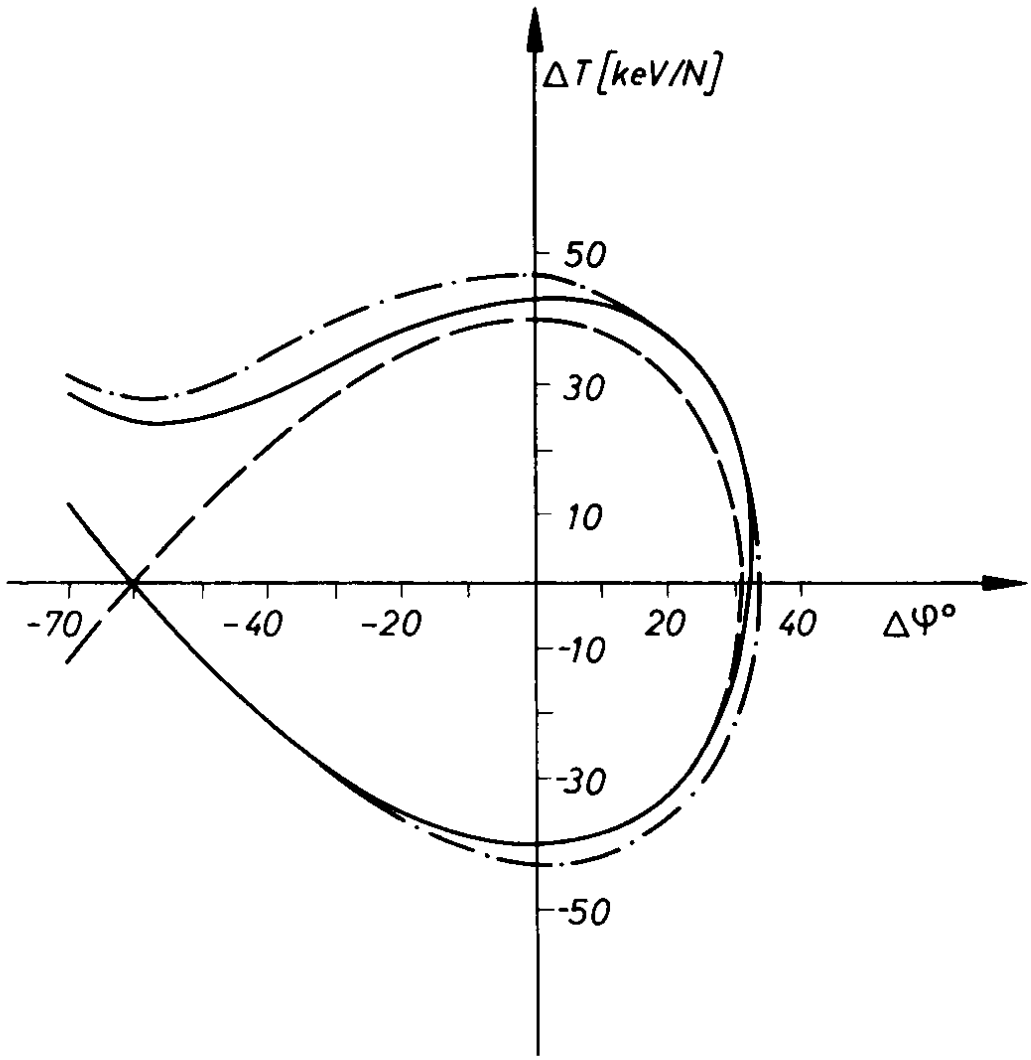

Fig. 9
Longitudinal acceptance of the poststripper accelerator for Uranium U^{25+}, $T_{initial}$=1.4 MeV/N

——— *Approximative calculation (stationary potentional method)*

——— *Exact computation, drift length 25 cm*

—·—·— *Exact computation, without drift lengths*

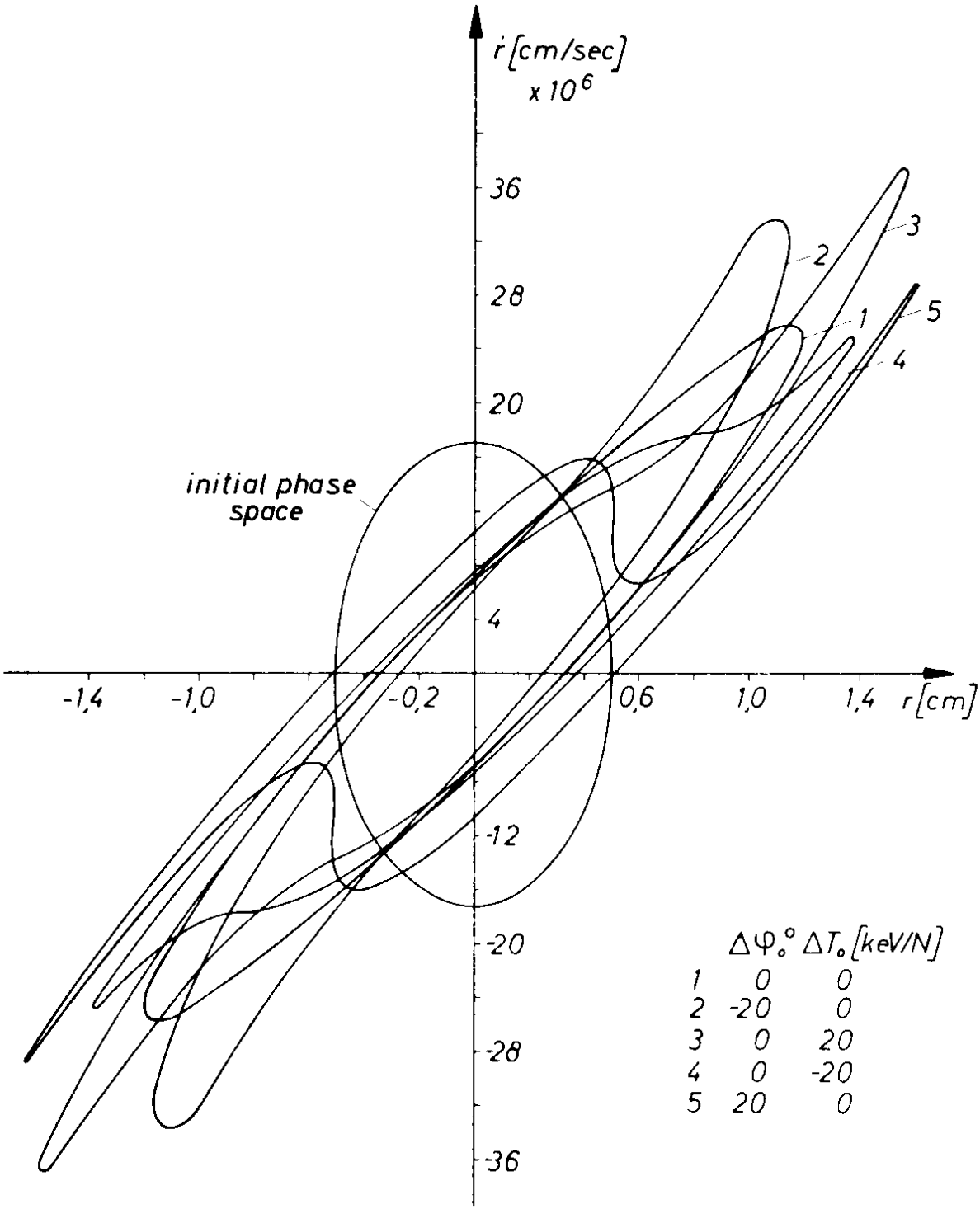

Fig. 10
Effect on transverse emittance of coupling to longitudinal motion
$T_{initial}$ = 1.4 MeV/N

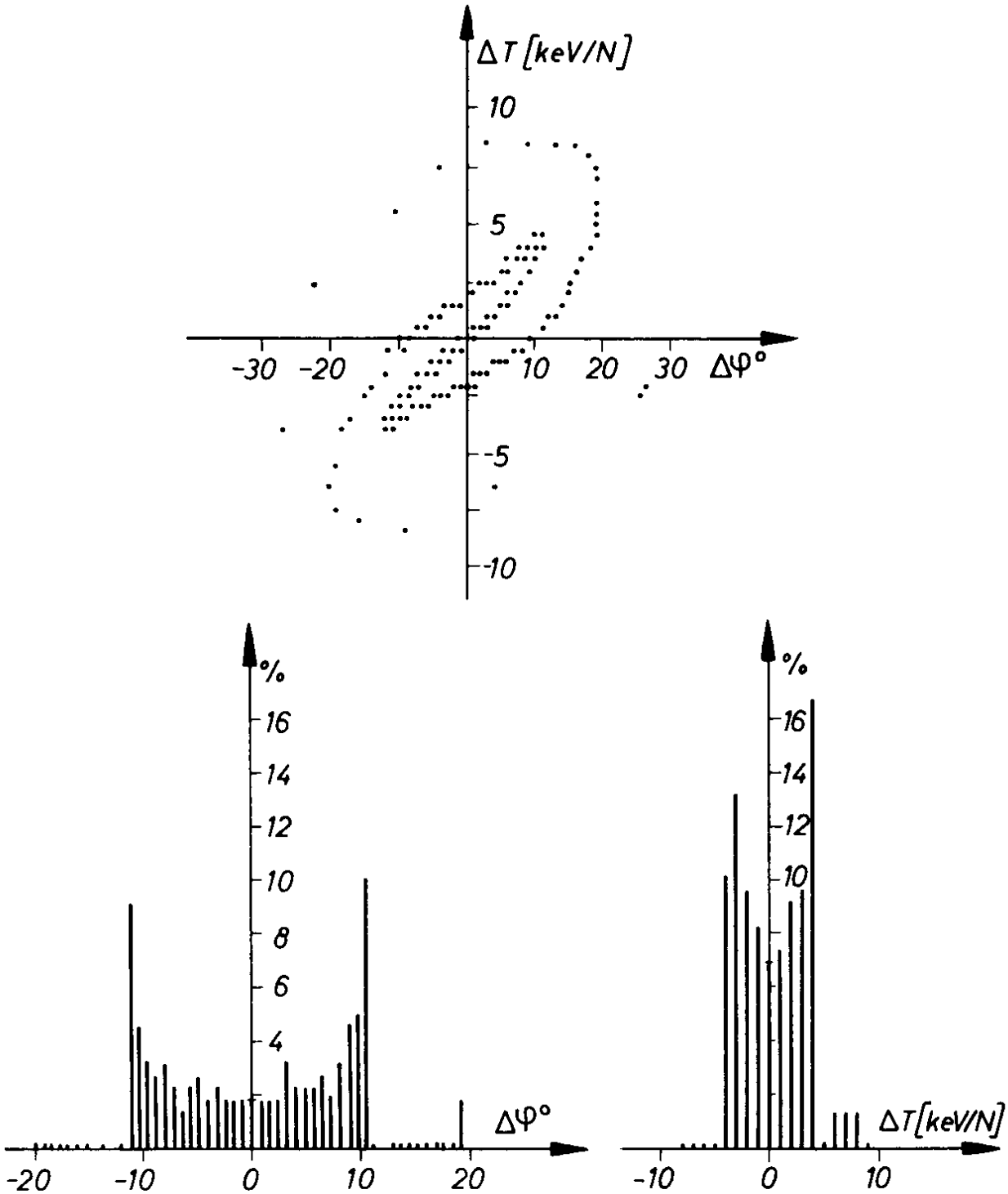

Fig.11a
Energy - phase space distribution and energy and phase spectra for uranium ions at 1.4 MeV/N

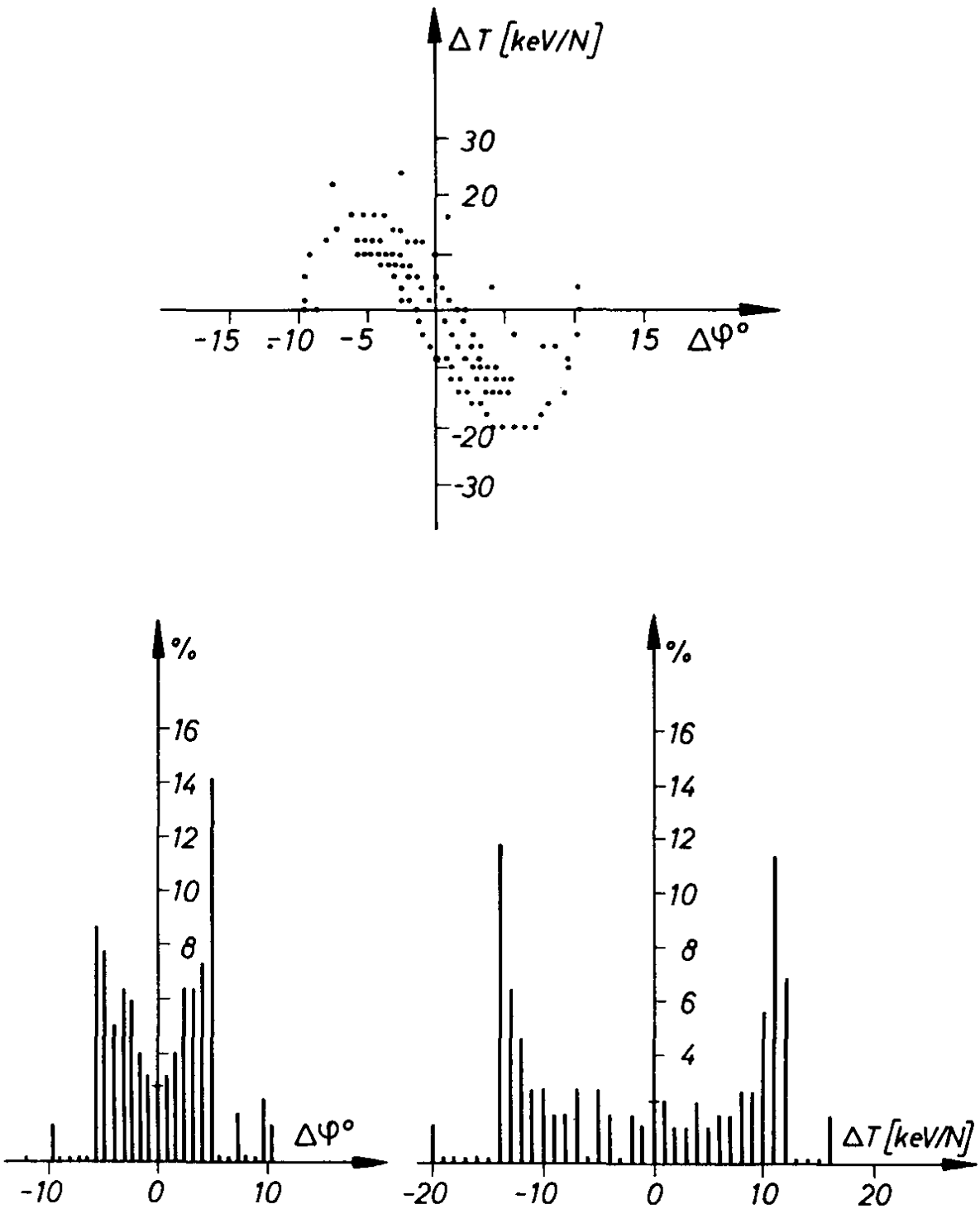

Fig. 11b
Energy - phase space distribution and energy and phase spectra for uranium ions at 7.0 MeV/N

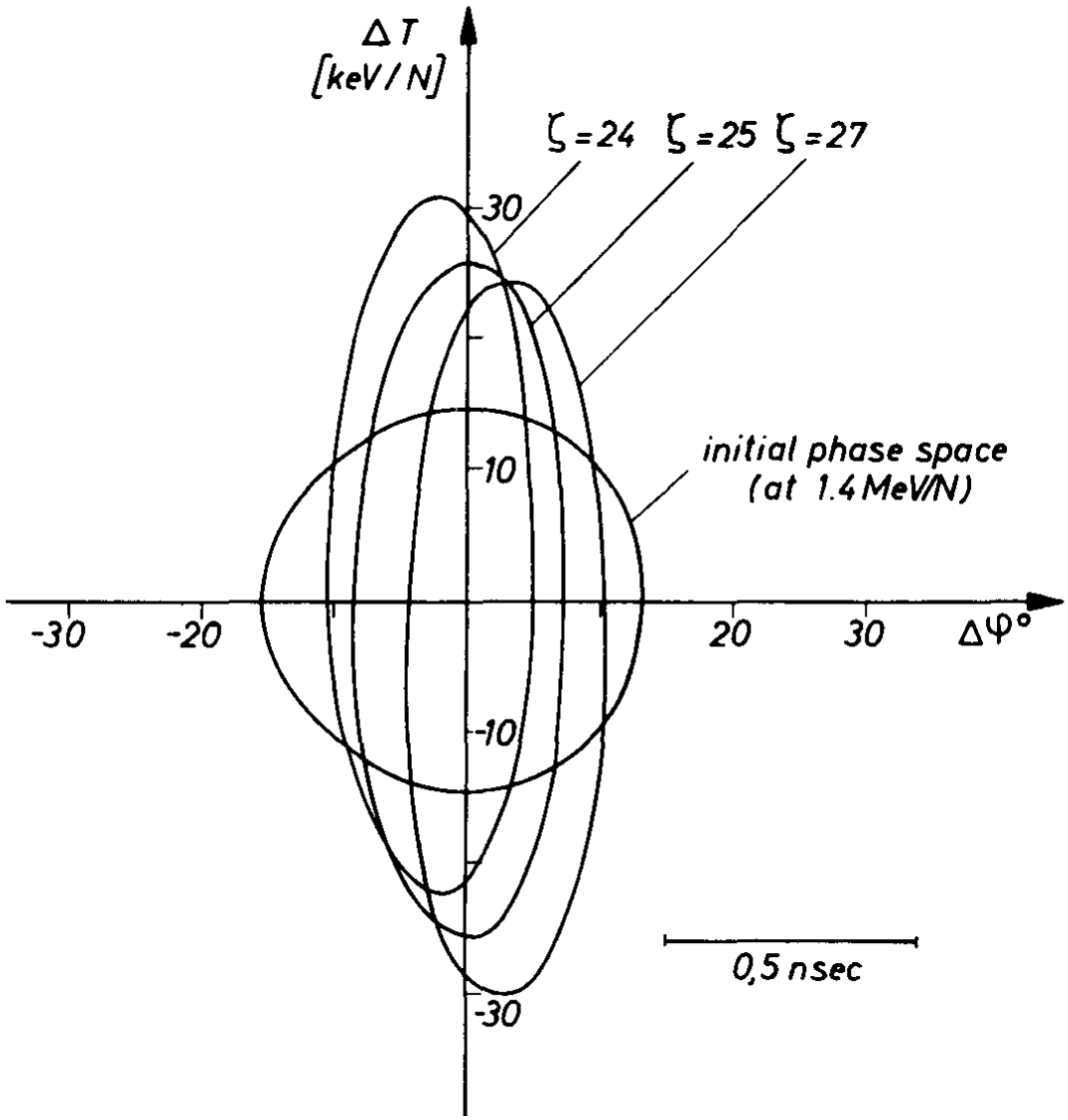

Fig. 12
Particle distribution in longitudinal phase space for uranium with single ($\zeta = 25$) or multiple ($\zeta = 24 - 27$) charge acceleration. Final energy is 7 MeV/N, linac is adjusted to U^{25+}.

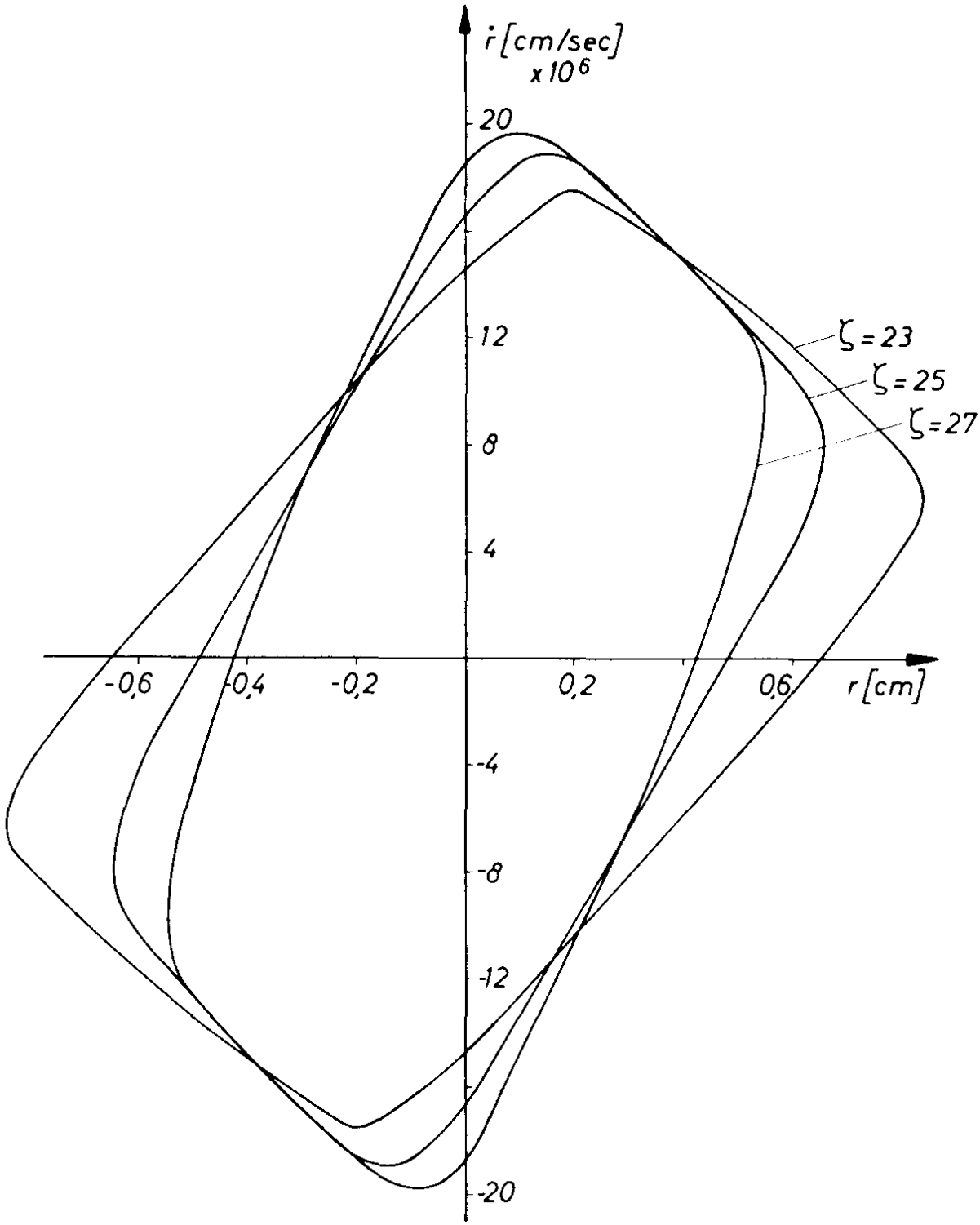

Fig. 13
Radial acceptance for various charge states at 1.4 MeV/N. Singulet N = 1 focusing, length of helix sections 1.0 m, effective length of qudrupoles 20cm, aperture 3cm. Poststripper linac is adjusted to U^{25+}.

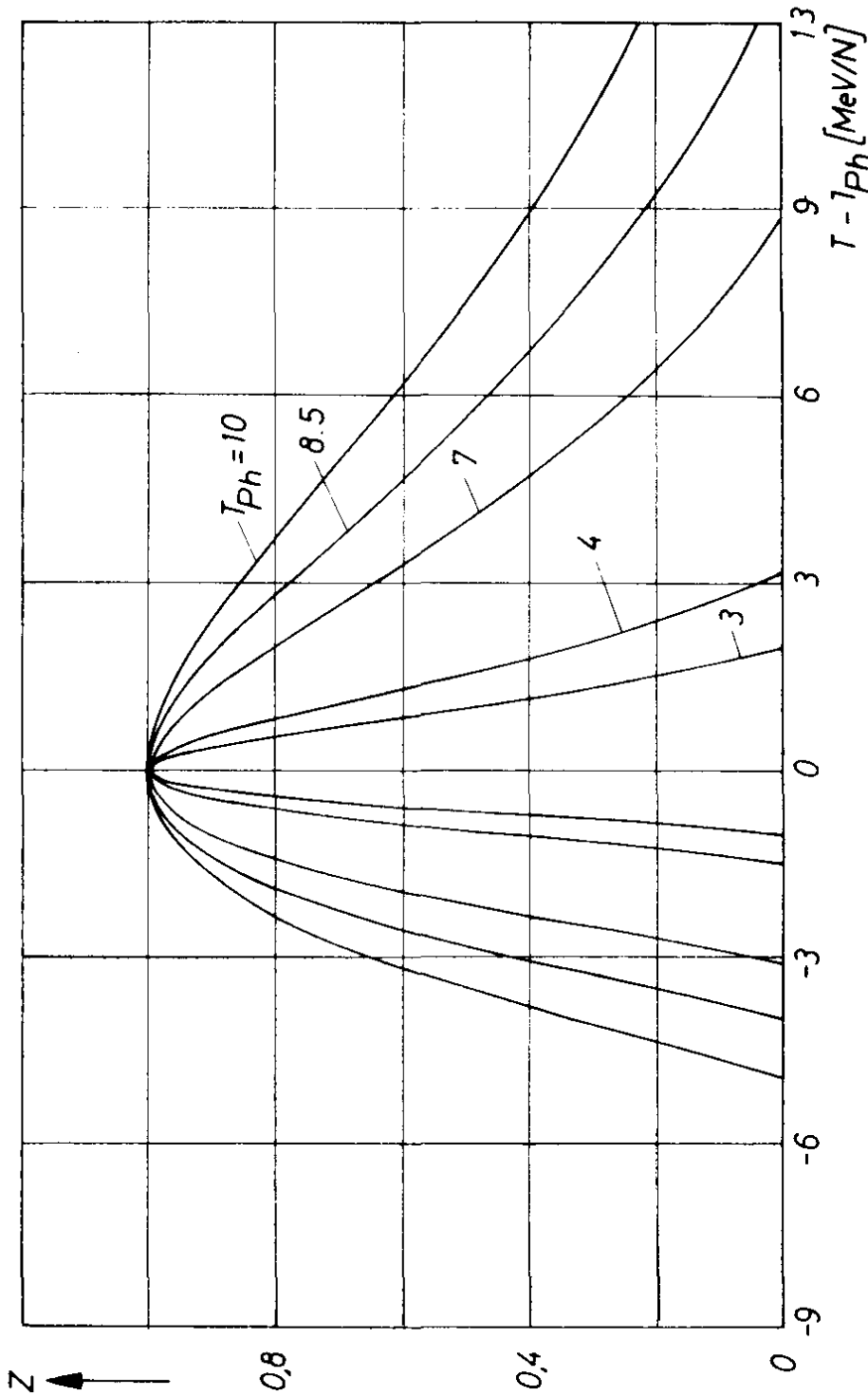

Fig. 14 a
Transit time factor for helix sections of different phase velocity versus relative particle energy
Helix length: 1.0 m, frequency 108.48 MHz

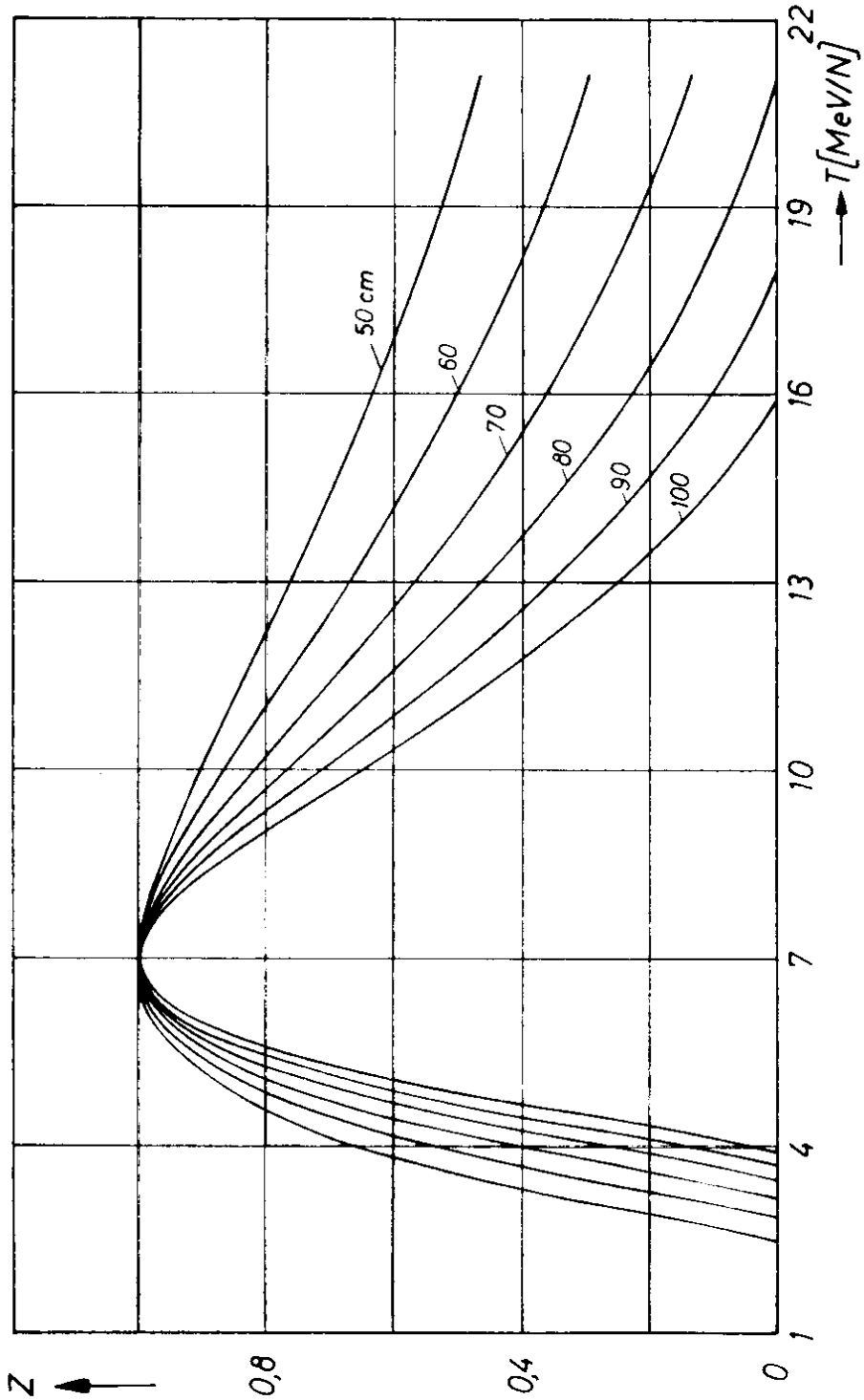

Fig. 14b
Transit time factor for helix sections of different length versus particle energy.
Phase velocity: $3.67 \cdot 10^9$ cm/sec (7 MeV/N)
Frequency: 108.48 MHz

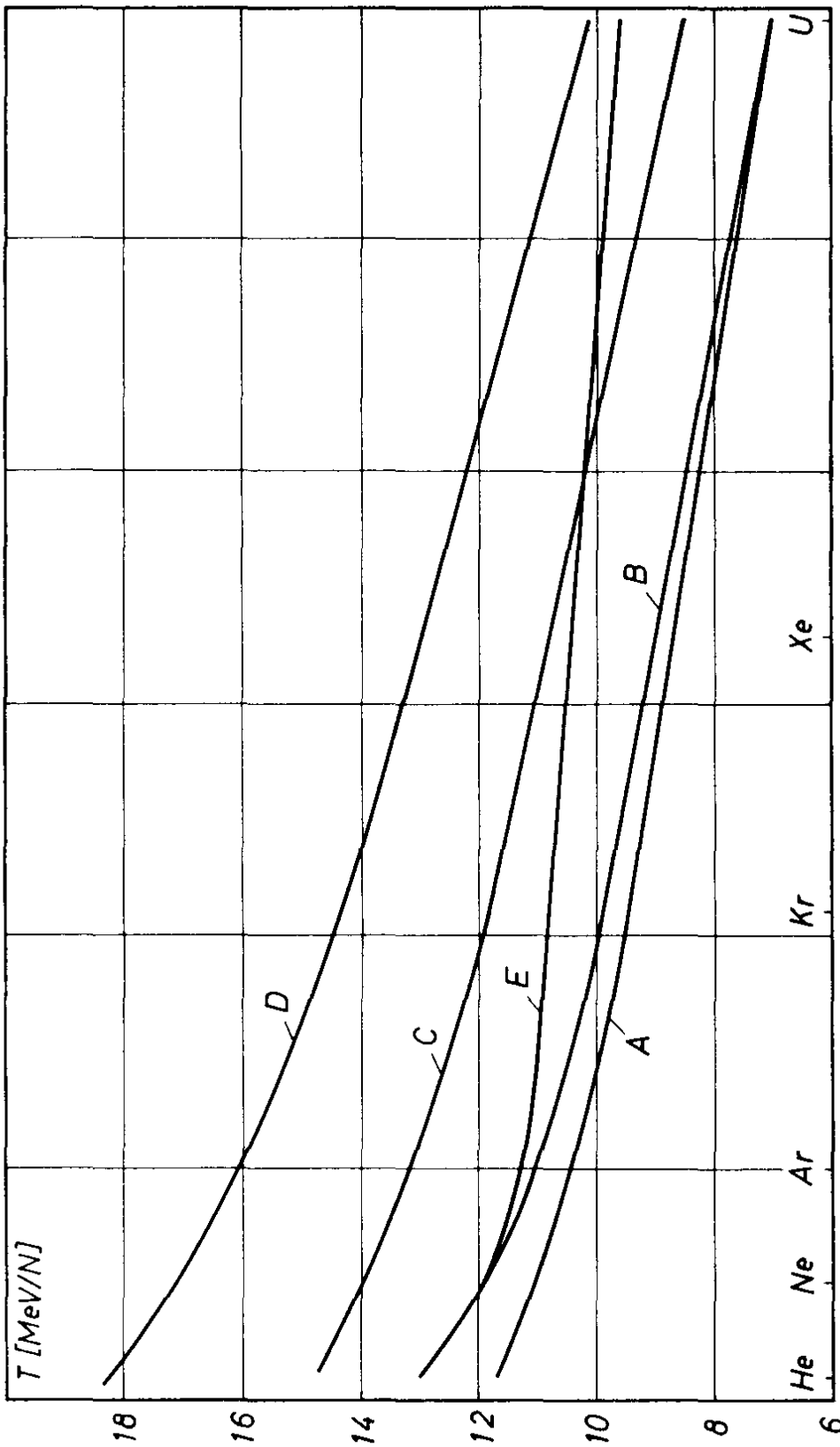

Fig. 15
Maximum energy versus atomic mass number A - D: Gasstripping at 1.4 MeV/N, E: Foil stripper at 1.4 MeV/N;
A, C, D, E: Length of helix sections 1.0 m throughout B: Length of last sections decreases from 1.0 m at 4.5 MeV/N to 0.6 m at 7 MeV/N.
Final energy for U^{25+}-Ions [MeV/N]: A, B, E: 7; C: 8.5; D: 10

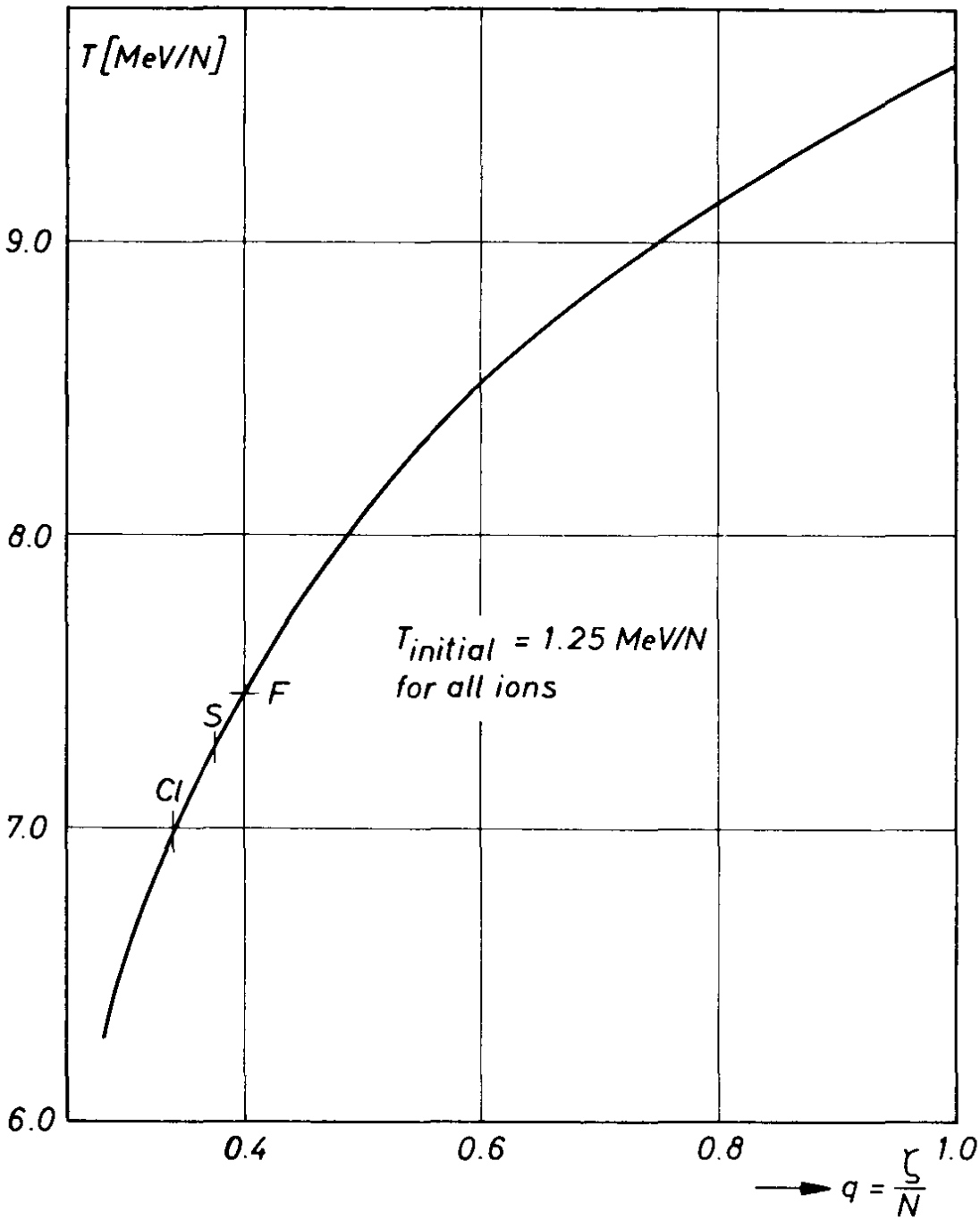

Fig. 16
Maximum energy versus specific ionisation
Bromine accelerator ($\zeta = 23$) $q_{min} = 0.284$
$T_i = 1.25$ MeV/N
$T_f = 6.28$ MeV/N